Journal of Solid State Chemistry 184 (2011) 2244–2249

Contents lists available at ScienceDirect

Journal of Solid State Chemistry

journal homepage: www.elsevier.com/locate/jssc

Enhanced visible-light absorption and dopant distribution of iodine-TiO_2 nanoparticles synthesized by a new facile two-step hydrothermal method

Xiaoting Hong [a], Zhiping Luo [b,1], James D. Batteas [c,*]

[a] School of Chemistry and Environment, South China Normal University, Guangzhou 510006, China
[b] Microscopy and Imaging Center, Texas A&M University, College Station, TX 77843, USA
[c] Department of Chemistry, Texas A&M University, College Station, TX 77842, USA

ARTICLE INFO

Article history:
Received 6 April 2011
Received in revised form
8 June 2011
Accepted 13 June 2011
Available online 21 June 2011

Keywords:
Doped TiO_2
Semiconducting nanoparticles
Light harvesting nanomaterials
Hydrothermal synthesis

ABSTRACT

In order to prepare visible-light responsive iodine-doped TiO_2, a new facile synthetic approach was proposed, which started with the cost-efficient and environmentally friendly precursor of undoped anatase TiO_2 to form nanotube structures as templates that collapsed and recrystallized into I-TiO_2 nanopowders in HIO_3 solution, followed by annealing at different temperatures. The modification of TiO_2 to incorporate iodine and form titanium dioxide with significantly enhanced absorption in the visible range of the spectrum was investigated. The extent of iodine dopant incorporation was determined by X-ray photoelectron spectroscopy (XPS) and energy dispersive X-ray analysis (EDX) and was found to be homogenously distributed on each nanostructure as determined by electron energy-loss spectroscopy (EELS) elemental mapping and EDX spectroscopy. The modified TiO_2 exhibits a dramatically extended absorption edge beyond 800 nm as compared to the original and unmodified TiO_2.

1. Introduction

Light harvesting materials for solar energy production have been extensively studied by surface modification of the existing well-known materials [1] or by exploring new types of materials [2,3]. TiO_2, a low-cost n-type semiconductor, has been of wide interest because of its versatile applications in areas such as photocatalysis [4–6], dye-sensitized solar cells (DSSCs) [7,8], sensors [9,10], and self-cleaning coatings [11,12]. As the bandgap of anatase TiO_2 is in the near-UV range of the electromagnetic spectrum, ca. 3.2 eV (285 nm), only UV light is able to create electron–hole pairs and to initiate photocatalytic processes [13]. As UV light constitutes only 5% of the solar spectrum, 95% of the solar photons are therefore useless for TiO_2 photocatalysis [14]. As such, any modifications of TiO_2 photocatalysts that result in an enhancement of visible-light absorption, or in the introduction of stable optical sensitizers, are expected to have a significant impact.

Numerous efforts have been made to improve the light-harvesting and photocatalytic efficiency of TiO_2, especially within the range of visible light. Aside from tuning the nanostructure of TiO_2 [15], different dopants have been widely utilized to enhance its response to visible light. One approach is the doping of TiO_2 with various transitions metals such as Bi, Ag, Fe, Ce, and V [4, 16–19]. Although many of these doped systems show enhanced photoactivity in the visible region of the spectrum, their efficiency is highly dependent on the method of preparation, and their application in some cases can be restricted by their thermal stability, the ability to precisely control the metal-oxide cluster size and distribution [20], and increases in carrier-recombination [21].

Doping of TiO_2 with nonmetals, such as N, S, F, C, Br, and Cl, have also been explored as means to improve performance [22–27]. It has previously been shown that a significant enhancement of visible light absorption can also be obtained by using iodine as a non-metal dopant for TiO_2 through the direct hydrolysis of tetrabutyl titanate in iodic acid solution [28]. The I-doped TiO_2 showed a markedly enhanced absorption in the visible spectrum and dramatically enhanced photocatalytic activity under visible light irradiation as compared to undoped TiO_2. As iodine-doped TiO_2 (I-TiO_2) has been successively developed by different methods, there is an obvious interest in the fundamental mechanisms responsible for light enhancement in the visible region. Computational studies by Long et al. [29] have examined the relationship between electronic structure and the enhanced visible light response of I-doped anatase TiO_2 from first-principles calculations using density functional theory. Tojo et al. [30], using time-resolved diffuse reflectance spectroscopy, revealed that the recombination of electron/hole pairs was inhibited because the I-doped sites acted as a traps site to capture the e^-.

Other groups have also reported the synthesis of I-TiO_2 by hydrothermal methods. Liu and co-workers [31] synthesized iodine-doped mesoporous titania with a bicrystalline (anatase and rutile) framework via a two-step template hydrothermal

* Corresponding author. Fax: +1 979 845 4719.
E-mail addresses: hanren.xiaoting@gmail.com (X.T. Hong), luo@mic.tamu.edu (Z. Luo), batteas@chem.tamu.edu (J.D. Batteas).
[1] Fax: +1 979 847 8933.

0022-4596/$ - see front matter © 2011 Elsevier Inc. All rights reserved.
doi:10.1016/j.jssc.2011.06.012

synthetic route. Multivalent iodine (I^{7+}/I^{-}) doped TiO_2 has also been prepared via a combination of deposition–precipitation process and hydrothermal treatment, where the iodine dopant was considered as a surface-adsorbed species, such as an IO_4 group [32]. There have also been reports of co-doping iodine-doped TiO_2 with other metal oxides, further shifting its response to visible light and improving its catalytic activity [33]. More recently, the absorption edge of I-TiO_2 has been extended up to ~800 nm. This absorption enhancement can generally be attributed to the distribution and occupation of localized states of iodine and their configuration on the surface, as exhibited in anatase TiO_2 with the co-existence of I–O–I and I–O–Ti structures [34].

While these experiments have presented various synthetic methods for creating visible light responsive iodine-doped TiO_2, they all required the use of expensive metal-organic precursors such as titanium tetraisopropoxide or tetrabutyl titanate [28,30,31,33], or highly toxic precursors (titanium tetrafluoride) [34] for the synthesis. Especially, as the fluoride solution was used in their study, any acid contamination would cause the higher toxicity due to the increasing amount of HF.

Here we have advanced the work in this area by developing a new synthetic approach for the formation of visible light responsive iodine-doped TiO_2 starting with the cost-efficient and environmentally friendly precursor of undoped anatase TiO_2 to first form titanate ($H_2Ti_3O_7$) nanotubes by a hydrothermal method [35]. Then, I-TiO_2 nanopowders were prepared by collapsing the titanate nanotubes in HIO_3 solution in a Teflon-lined autoclave, followed by annealing. The absorption edge of the as-synthesized anatase I-TiO_2 single crystalline nanostructures notably extends to >800 nm and increases with annealing temperature. To our knowledge, using undoped TiO_2 nanoparticles as the precursor to synthesize non-metal doped TiO_2 nanoparticles has not been previously reported. Herein, we describe the new facile synthetic route, dopant distribution of the doped materials, and materials characterization.

2. Experimental

2.1. Materials synthesis

Titanate nanotubes were first produced using a hydrothermal synthetic method with successive acid washing and heat treatment [35]. Here, 0.2 g of commercial anatase TiO_2 granules (99.9%, Alfa, USA) was first dispersed in 20 ml of 10 M NaOH aqueous solution and moderately stirred for 2 h in air. The mixture was then placed into a custom-made Teflon-lined autoclave of ~30 ml capacity. The autoclave was sealed and maintained in an oven at 150 °C under autogenous pressure for 24 h and then cooled to room temperature naturally.

The resulting nanostructure products were alternatively washed with HCl solution (~1 M) and high purity water (18.2 MΩ cm, Barnstead) at least three times and collected by centrifugal separation. The as-synthesized titanate nanotubes were then soaked in 15 mL ~1 M HCl solution for ~24 h. The titanate nanotubes were rewashed with HCl solution (~1 M) and high purity water until neutral and dried in an oven at 100 °C for ~7 h after centrifugal separation. A portion of the dried $H_2Ti_3O_7$ nanotubes (0.15 g) were dispersed in 10 mL HIO_3 solution (0.15 g HIO_3) and transferred into the Teflon-lined autoclave at 110 °C for 12 h. The iodic acid modified products were then dried at 100 °C for ~7 h and the dried products were finally annealed at 350, 450, and 550 °C for 2 h in air, respectively, with a heating rate of 120 °C/h. A schematic description of the synthetic route of I-doped TiO_2 from undoped TiO_2 is shown in Fig. 1. Undoped TiO_2 materials were also prepared under the same experimental conditions and used as a reference at the different temperatures.

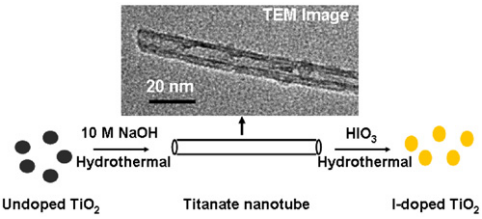

Fig. 1. Schematic description of the synthetic route of I-doped TiO_2 from undoped TiO_2.

2.2. Characterization

The sample phases were measured using a conventional powder X-ray diffractometer (XRD, BRUKER D8-Focus Bragg–Brentano) with Cu Kα radiation. They were also investigated using transmission electron microscopy and selected area electron diffraction (TEM and SAED, JOEL JEM-2010 and FEI Tecnai G^2 F20, both 200 kV). The latter instrument was equipped with a high-angle annular dark-field (HAADF) detector for *Z*-contrast imaging and energy dispersive X-ray (EDX) analysis using a nanobeam of 1 nm in the scanning transmission electron microscopy (STEM) mode, and a post-column Gatan Image Filter for EELS studies. Surface analysis of the samples was also performed using X-ray photoelectron spectroscopy (XPS) using a Kratos AXIS ULTRA X-ray photoelectron spectrometer equipped with a 165 mm hemispherical electron energy analyzer with a monochromated Al Kα source. Absorption spectra of the different TiO_2 nanopowders were measured with a Hitachi U-4100 UV/VIS/NIR spectrophotometer with an integrated sphere system. Raman microspectroscopy measurements were made with a WITec confocal Raman microscope (alpha 300) using an air cooled Ar ion laser (488 nm) for the excitation, and collected with a Nikon 100×, 0.9 NA objective, onto a Peltier cooled CCD detector (Andor) with a Acton triple grating spectrometer with a spectral resolution of 0.24 cm^{-1}.

3. Results and discussion

3.1. X-ray powder diffraction

The crystalline structure of iodine-doped TiO_2 is nearly independent to the annealing process. Almost all peaks on the XRD patterns of the different iodine-doped and reference TiO_2 samples (see Fig. 2) were assigned to the anatase crystalline phase without any dopant related crystalline phases under the conditions analyzed. As the annealing temperature was increased, a very faint amount of rutile crystalline phases appeared at 450 and 550 °C. Also, the crystallinity of the I-TiO_2 specimens significantly increased with temperature. The average particle size of the crystalline I-TiO_2 was determined from the width of the XRD peaks using the Scherrer equation [36], and was estimated to be ~7, ~11, and ~14 nm at 350, 450, and 550 °C, respectively.

3.2. Transmission electron microscopy

As mentioned above, the I-TiO_2 nanoparticle size slightly increases with annealing temperature. From the measurement of ca. 100 independent zero-loss TEM images such as those in Fig. 3, the average grain size of I-TiO_2 (350 °C), I-TiO_2 (450 °C) and I-TiO_2 (550 °C) was roughly confirmed to be about 9, 14 and 16 nm, respectively, consistent with the aforementioned estimations from the Scherrer equation. HRTEM images shown in Fig. 3a–c illustrate that the I-TiO_2 nanopowders are single crystal in nature, with a lattice spacing of 0.35 nm, which corresponds to the lattice

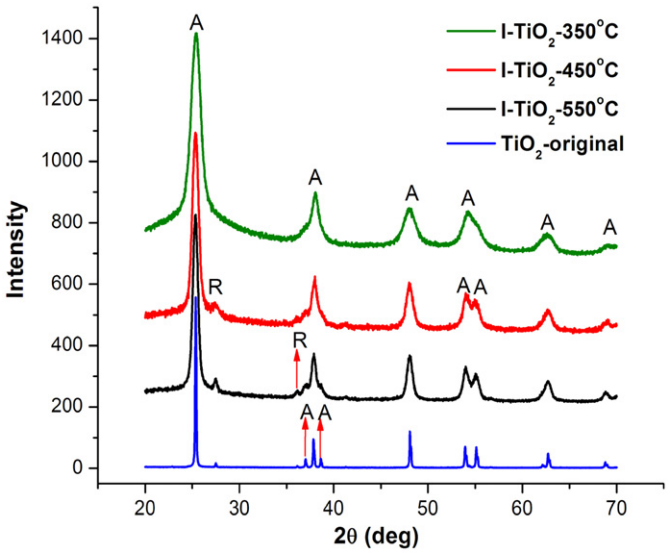

Fig. 2. XRD patterns of undoped TiO_2 and as-synthesized I-TiO_2 nanoparticles calcined at 350, 450, and 550 °C for 2 h. The letters A and R correspond to the anatase and rutile phase structures, respectively.

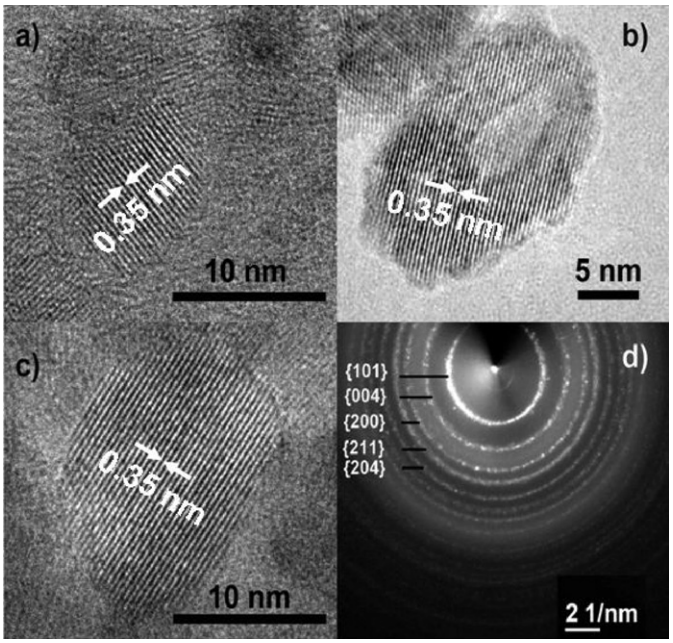

Fig. 3. HRTEM images of I-TiO_2 (350 °C) (a), I-TiO_2 (450 °C) (b) and I-TiO_2 (550 °C) (c) and selected diffraction pattern of I-TiO_2 (450 °C) (d).

spacing of the (1 0 1) plane of the anatase phase. Furthermore, the representative SAED pattern of I-TiO_2 (450 °C) shown in Fig. 3d also indicates that the I-TiO_2 nanoparticles have an anatase phase lattice structure, consistent with the XRD measurements.

The distribution of the iodine dopant in the specimens was also examined by EELS elemental mapping. Shown in the second row of Fig. 4 are elemental maps from the M-shell electrons (619 eV) of iodine, while the third and the fourth rows of Fig. 4 show the elemental maps from the K-shell electrons of oxygen (532 eV) and L-shell electrons of titanium (462 eV), respectively. All of the maps were acquired using a standard three-window method. By comparing these spectral maps to the corresponding zero-loss TEM images, we see the dopant distribution was homogenous in the I-TiO_2 nanoparticles. The relatively low contrast of the iodine maps is indicative of the low concentration of I in the TiO_2

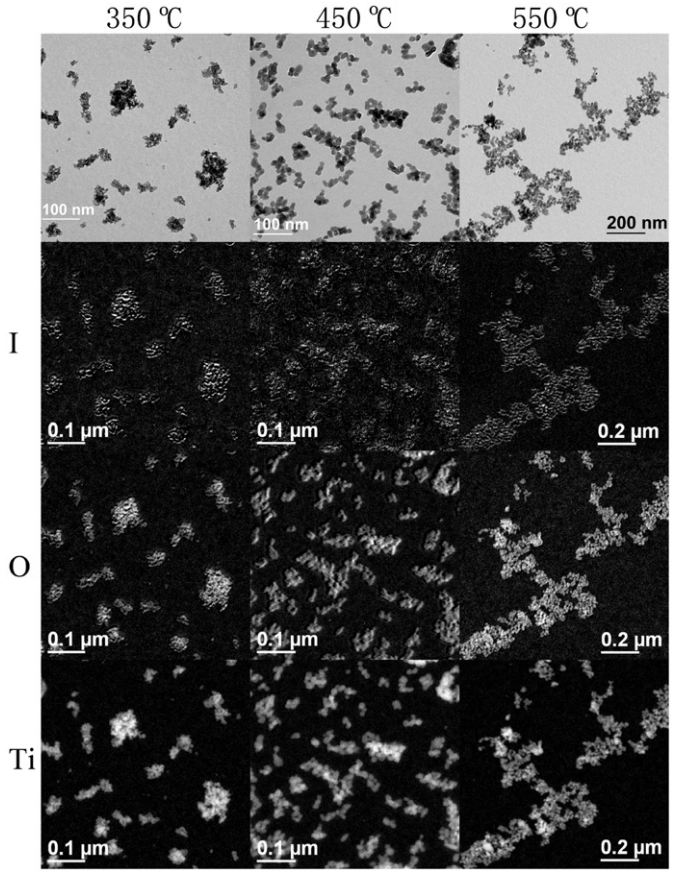

Fig. 4. Zero-loss images (1st row) and EELS elemental maps of iodine (2nd row), oxygen (3rd row) and titanium (4th row) of I-TiO_2 (350 °C), I-TiO_2 (450 °C), and I-TiO_2 (550 °C).

nanostructures, as compared to oxygen and titanium, which was consistent with the energy dispersive X-ray spectroscopy results (Fig. 5). The atomic percentages of iodine of I-TiO_2 (350 °C), I-TiO_2 (450 °C), and I-TiO_2 (550 °C) were estimated to be 2.2 ± 0.3, 1.1 ± 0.1, and 0.7 ± 0.1%, respectively.

In Fig. 5, it was found that all samples contained trace amounts of sodium and phosphorus as reported elsewhere [37,38], which may be due to the residual from sodium titanate nanotubes, impurities associated with the reactant carrier lines in the experimental setup, impurities of the reactants in general, or the TEM specimen holder. The incorporation of iodine did not appear to result in any significant change in the average unit cell dimension, as the bond length of I–O (2.04 Å) is close to the Ti–O bond (1.93 Å) [34], and the iodine atomic radius (0.62 Å) is also close to that of titanium (0.64 Å) [28], which is consistent with the insignificant changes in the crystalline structure.

The iodine-doped TiO_2, annealed to at 450 °C, was also examined by STEM *Z*-contrast imaging using the HAADF detector on the microscope. In these measurements, an element with a higher atomic number exhibits brighter contrast as compared to lighter elements with lower atomic number. The STEM image, along with a line scan with a beam size of 1 nm, is shown in Fig. 6. The line profiles of the STEM image intensity, and the EDX signals of Ti, O, and I are shown in Fig. 6(b). Note the much lower EDX counts for I as compared to those of Ti and O in these profiles and the one-to-one correspondence between the peak positions. Larger nanoparticle aggregates, at a position of ~40 and ~160 nm, contributed high EDX intensities for each element, while the single nanoparticles at positions of ~95 and ~390 nm showed a relatively low intensity; this implies that the elemental distributions of Ti, O,

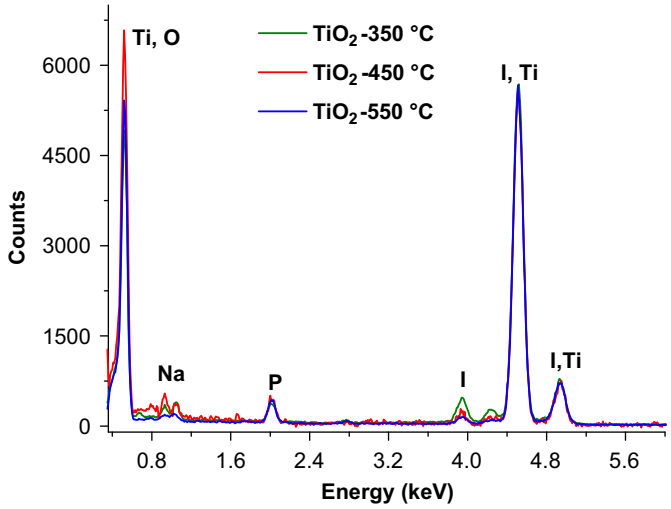

Fig. 5. EDX spectra of I-TiO_2 nanopowders calcined at 350, 450, and 550 °C.

and I are homogeneous within the particles, regardless of nanoparticle size and location, and clearly indicates the presence of the titanium dioxide and dopant iodine.

3.3. X-ray photoelectron spectroscopy

In the XPS measurements, the binding energies were corrected using the adventitious carbon contamination peak at 284.5 eV C(1*s*) [39]. The XPS spectra of the I (3*d*) region in Fig. 7 show two doublet peaks at [623.6 eV I($3d_{5/2}$) and 635.1 eV I($3d_{3/2}$)] and [624.2 eV I($3d_{3/2}$) and 635.6 eV I($3d_{5/2}$)] for HIO_3 and I-TiO_2 (350, 450, and 550 °C), respectively. After the doping, the main peak of iodine in I-TiO_2 (624.2 eV) was 0.6 eV higher than that in the HIO_3 (623.6 eV), which agrees well with previous reports [30]. The shift of the XPS peaks to higher binding energy can be ascribed to the substitution of Ti^{4+} by the dopant (in this case cationic I^{5+}), which is energetically favorable due to their near equivalent ionic radius and to that fact that the dopant of iodic acid has analogous perovskite structure to TiO_2. Substitution for O is unlikely as the XPS peak position for I^- (in NaI for example) is ~618.4 eV [40]. This exchange mechanism has been suggested previously both experimentally [28] and theoretically based on density functional theory calcaultions [30]. Upon doping, the creation of Ti^{3+} and oxygen vacancies might happen during the calcination process while maintaining charge neutrality of the iodine-doped TiO_2 [41]. Moreover, as shown by the changes of the peak intensity in the XPS spectra, the content of the dopant iodine decreases with the annealing temperature, consistent with the results of the EDX spectra.

3.4. UV/VIS/NIR spectrophotometry

All of the doped TiO_2 nanomaterials showed a yellow to brown/orange color, suggesting their ability to absorb light in the visible region. UV–visible absorption spectra (Fig. 8) of the iodine-doped TiO_2 nanomaterials exhibit a significant broadening in the absorption compared to the red from that of undoped TiO_2. The mechanism of the enhanced absorption in visible light spectrum of doped TiO_2 is still under debate. Previous groups have proposed that midgap states and bandgap narrowing produce the resulting changes in absorption [42–44]. However, this explanation is controversial and lacks sufficient experimental evidence. Recently, Serpone [45,46] has provided a large body of evidence attributing the enhanced absorption of visible light in doped TiO_2 to the formation of oxygen vacancies and to the advent of the Ti^{3+} color centers induced by dopants, which is currently widely used for most research. The iodine-doped TiO_2

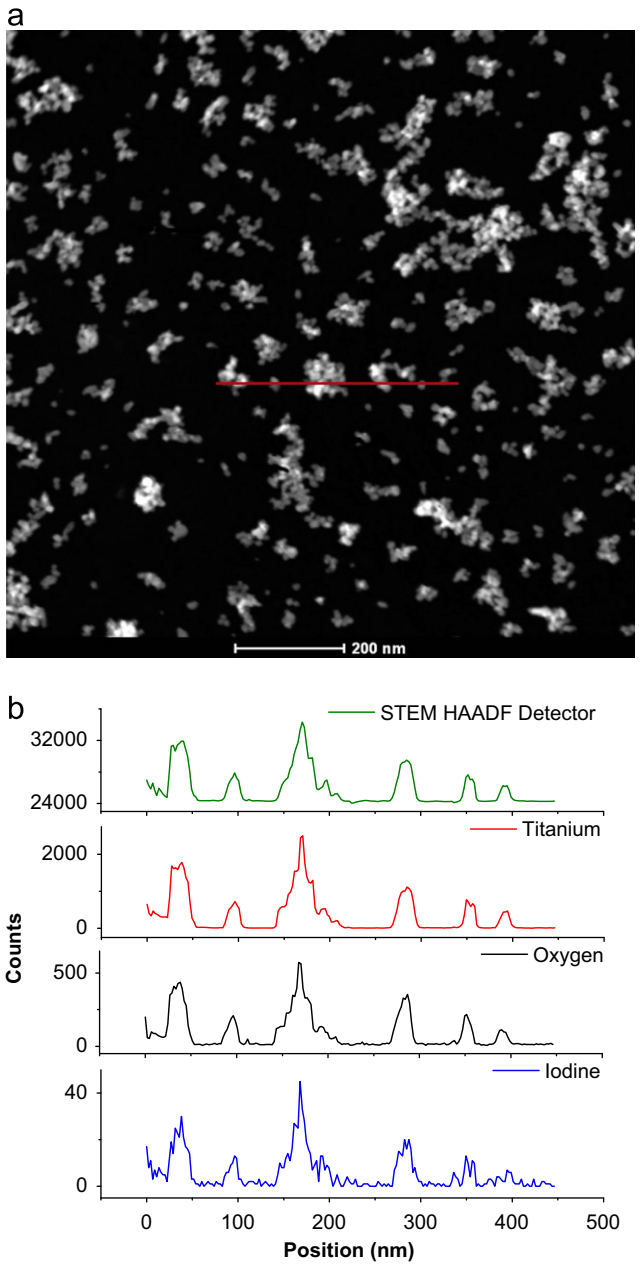

Fig. 6. (a) Scanning transmission electron microscopy (STEM) image of I-TiO_2 (450 °C). (b) Corresponding EDX line scan profiles of the region as shown in the STEM image (iodine, oxygen, and titanium).

nanomaterials annealed at 350, 450, and 550 °C, showed edge absorptions around ~414, ~424, and ~450 nm, respectively, while the undoped TiO_2 showed an absorption edge ~390 nm, which is typical for the anatase phase. The edge absorption difference can be attributed to the dopant concentration, the crystallinity, and the nanoparticle size. Compared to pure TiO_2, the additional absorption of iodine-doped nanomaterials was significantly extended to about 800 nm. Among the three I-TiO_2 samples, the changes in the optical properties decrease with the dopant concentration (from 350 to 550 °C), which is ascribed to the decrease of oxygen vacancies induced by excessive doping [47].

3.5. Raman spectroscopy

Fig. 9 shows the Raman shift of the I-TiO_2 and original TiO_2 nanomaterials. The Raman spectra of the nanomaterials were

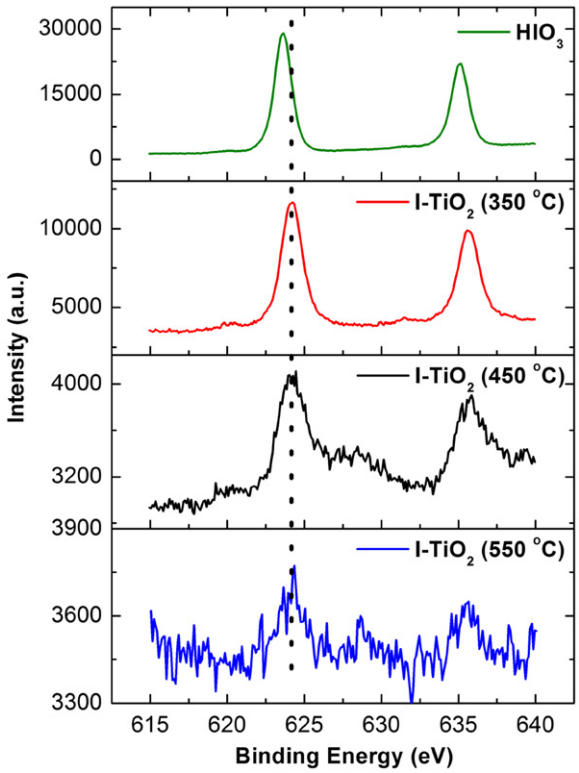

Fig. 7. I 3*d* high-resolution XPS spectra of HIO_3 and iodine-doped TiO_2 calcined at 350, 450, and 550 °C for 2 h.

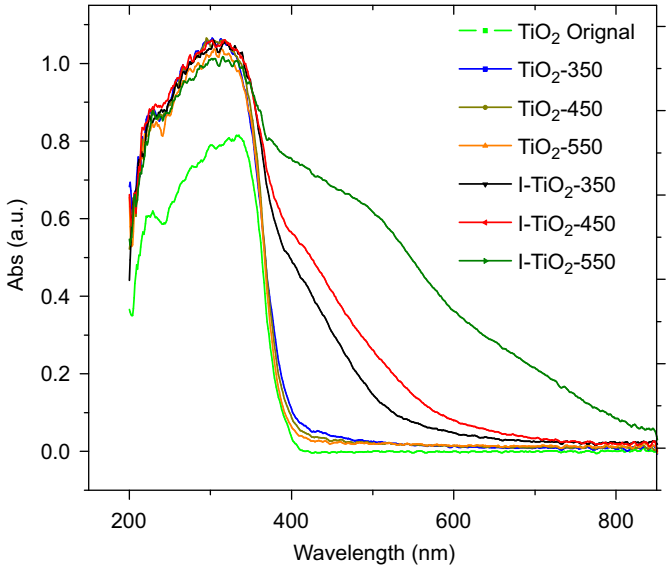

Fig. 8. UV–visible absorption spectra of original TiO_2, nondoped TiO_2, and iodine-doped TiO_2.

measured with an Ar ion laser, with a wavelength of 488 nm. In Fig. 9, the three peaks located at 394 (B_{1g}), 514 (A_{1g}), and 637 cm^{-1} (E_g) indicate that the original TiO_2 consisted of only the anatase crystal structure [1]. After iodine doping, the nanomaterial structures were found to remain in the anatase single crystal phase, independent of the annealing temperature. The results of the Raman studies show the existence of the anatase phase as the major phase, and that the rutile phase is negligible for all nanomaterials, consistent with the previous observations from XRD and HRTEM measurements.

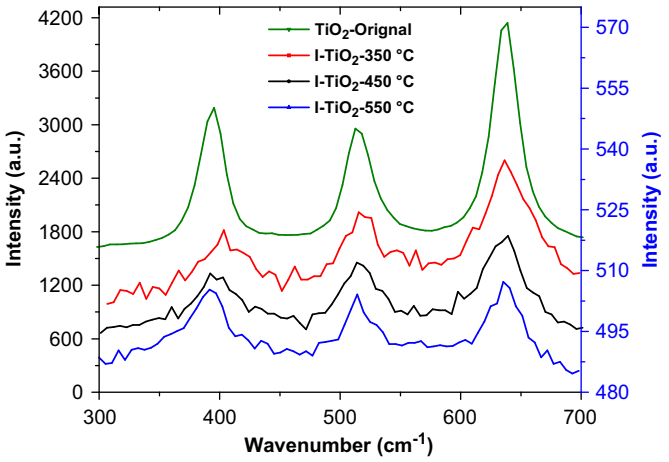

Fig. 9. Raman spectra of TiO_2-orignal and I-TiO_2 (350, 450, and 550 °C) (left *Y*-axis for TiO_2-original, right *Y*-axis for I-TiO_2).

4. Conclusions

In this work, we have prepared iodine-doped TiO_2 nanopowders using a new two-step hydrothermal synthetic method. Starting from an inexpensive and non-toxic precursor used for commercial TiO_2 nanocolloids, iodine-doped TiO_2 nanostructures were formed through iodine incorporation during the course of the collapse of intermediate titanate nanotubes. Anatase single crystalline nanostructures of I-TiO_2 were obtained after annealing up to 550 °C as confirmed from XRD, HRTEM and Raman microspectroscopy. Markedly enhanced visible-light absorption was observed in these lightly iodine-doped TiO_2 nanostructures as compared to the unmodified and original starting nanomaterials. EELS elemental mapping and STEM EDX measurements were systematically used to investigate the dopant distribution for the as-synthesized I-TiO_2. From these measurements, the iodine dopant was found to yield a homogenous distribution on each nanoparticle, and its content was quantized by EDX analysis. A key difference in our I-doped TiO_2 samples, and those previously reported in the literature is that that these materials exhibit a much more extended absorption edge up to 800 nm, with significant absorption in the 600–800 nm range [31,32]. While similar in nature to I-doped TiO_2 samples synthesized using titanium tetrafluoride and HIO_4 acid as precursor and dopant [35], in this case a much more significant absorption in the visible region of the spectrum is observed compared to these other systems. We expect that this two-step hydrothermal synthetic method from undoped TiO_2 to I-doped TiO_2 nanoparticle, with an intermediate stage of titanate nanotube, should be adaptable for the synthesis of other doped TiO_2, or of other materials with different doping sources.

Acknowledgments

J.D.B. acknowledges support for this work from the U.S. National Science Foundation (CHE-0848786) and the TAMU Energy Resources Program.

References

[1] S.M. Prokes, J.L. Gole, X. Chen, C. Burda, W.E. Carlos, Adv. Funct. Mater. 15 (2005) 161–167.
[2] D. Chen, J. Ye, Chem. Mater. 19 (2007) 4585–4591.
[3] X. Zhang, Z. Jin, Y. Li, S. Li, G. Lu, J. Colloid Interface Sci. 333 (2009) 285–293.
[4] L. Cui, Y. Wang, M. Niu, G. Chen, Y. Cheng, J. Solid State Chem. 182 (2009) 2785–2790.

[5] R. Kun, S. Tarján, A. Oszkó, T. Seemann, V. Zöllmer, M. Busse, I. Dékány, J. Solid State Chem. 182 (2009) 3076–3084.
[6] J. Jitputti, S. Pavasupree, Y. Suzuki, S. Yoshikawa, J. Solid State Chem. 180 (2007) 1743–1749.
[7] A. Kitiyanan, S. Ngamsinlapasathian, S. Pavasupree, S. Yoshikawa, J. Solid State Chem. 178 (2005) 1044–1048.
[8] C. Yu, J. Park, J. Solid State Chem. 183 (2010) 2268–2273.
[9] S. Santangelo, G. Messina, G. Faggio, A. Donato, L. De Luca, N. Donato, A. Bonavita, G. Neri, J. Solid State Chem. 183 (2010) 2451–2455.
[10] D. Morris, R.G. Egdell, J. Mater. Chem. 11 (2001) 3207–3210.
[11] W.S. Tung, W.A. Daoud, J. Colloid Interface Sci. 326 (2008) 283–288.
[12] J.H. Johnston, A.C. Small, J. Mater. Chem. 21 (2011) 1240–1243.
[13] W. Aaron, Chem. Mater. 5 (1993) 280–283.
[14] S. Yin, Q.W. Zhang, F. Saito, T. Sato, Chem. Lett. 52 (2003) 358–359.
[15] K. Varghese, M. Paulose, T.J. LaTempa, C.A. Grimes, Nano Lett. 9 (2009) 731–737.
[16] C. Liu, X. Tang, C. Mo, Z. Qiang, J. Solid State Chem. 181 (2008) 913–919.
[17] H. Žabová, J. Sobek, V. Církva, O. Šolcová, Š. Kment, M. Hájek, J. Solid State Chem. 182 (2009) 3387–3392.
[18] S. Sajjad, S.A.K. Leghari, F. Chen, J. Zhang, Chem. Eur. J. 16 (2010) 13795–13804.
[19] J. Choi, H. Park, M.R. Hoffmann, J. Phys. Chem. C 114 (2010) 783–792.
[20] W. Choi, A. Termin, M.R. Hoffmann, J. Phys. Chem. 98 (1994) 13669–13679.
[21] H. Yamashita, M. Honda, M. Harada, Y. Ichihashi, M. Anpo, T. Hirao, N. Itoh, N. Iwamoto, J. Phys. Chem. B 102 (1998) 10707–10711.
[22] S. Livraghi, A.M. Czoska, M.C. Paganini, E. Giamello, J. Solid State Chem. 182 (2009) 160–164.
[23] W. Ho, J.C. Yu, S. Lee, J. Solid State Chem. 179 (2006) 1171–1176.
[24] J.G. Yu, J.C. Yu, B. Cheng, S.K. Hark, K. lu, J. Solid State Chem. 174 (2003) 372–380.
[25] S. Yin, Y. Aita, M. Komatsu, J. Wang, Q. Tang, T. Sato, J. Mater. Chem. 15 (2005) 674–682.
[26] H. Luo, T. Takata, Y. Lee, J. Zhao, K. Domen, Y. Yan, Chem. Mater. 16 (2004) 846–849.
[27] H. Xu, Z. Zheng, L. Zhang, H. Zhang, F. Deng, J. Solid State Chem. 181 (2008) 2516–2522.
[28] X.T. Hong, Z.P. Wang, W.M. Cai, F. Lu, J. Zhang, Y.Z. Yang, N. Ma, Y.J. Liu, Chem. Mater. 17 (2005) 1548–1552.
[29] M.C. Long, W.M. Cai, Z.P. Wang, G.Z. Liu, Chem. Phys. Lett. 420 (2006) 71–76.
[30] S. Tojo, T. Tachikawa, M. Fujitsuka, T. Majima, J. Phys. Chem. C 112 (2008) 14948–14954.
[31] G. Liu, Z. Chen, C. Dong, Y. Zhao, F. Li, G.Q. Lu, H.M. Cheng, J. Phys. Chem. B 110 (2006) 20823–20828.
[32] W. Su, Y. Zhang, Z. Li, L. Wu, X. Wang, J. Li, X. Fu, Langmuir 24 (2008) 3422–3428.
[33] Z. He, X. Xu, S. Song, L. Xie, J. Tu, J. Chen, B. Yan, J. Phys. Chem. C 112 (2008) 16431–16437.
[34] G. Liu, C. Sun, X. Yan, L. Cheng, Z. Chen, X. Wang, L. Wang, S.C. Smith, G.Q. Lu, H.M. Cheng., J. Mater. Chem. 19 (2009) 2822–2829.
[35] T. Kasuga, M. Hiramatsu, A. Hoson, T. Sekino, K. Niihara, Langmuir 14 (1998) 3160–3163.
[36] J.C. Yu, L.Z. Zhang, J.G. Yu, Chem. Mater. 14 (2002) 4647–4653.
[37] H. Choi, A.C. Sofranko, D.D. Dionysiou., Adv. Funct. Mater. 16 (2006) 1067–1074.
[38] N.F. Fahim, T. Sekino, Chem. Mater. 21 (2009) 1967–1974.
[39] J.M. Song, Y.Z. Lin, H.B. Yao, F.J. Fan, X.G. Li, S.H. Yu, ACS Nano 3 (2009) 653–660.
[40] P.M.A. Sherwood, J. Chem. Soc. Faraday Trans. II 72 (1976) 1805–1820.
[41] R. Bechstein, M. Kitta, J. Schütte, A. Kühnle, H. Onishi, J. Phys. Chem. C 113 (2009) 3277–3280.
[42] R. Asahi, T. Morikawa, T. Ohwaki, K. Aoki, Y. Taga, Science 293 (2001) 269–271.
[43] P.G. Wu, C.H. Ma, J.K. Shang, Appl. Phys. A: Mater. Sci. Process. 81 (2005) 1411–1417.
[44] T.C. Jagadale, S.P. Takale, R.S. Sonawane, H.M. Oshi, S.I. Patil, B.B. Kale, S.B. Ogale, J. Phys. Chem. C 112 (2008) 14595–14602.
[45] N. Serpone, J. Phys. Chem. B 110 (2006) 24287–24293.
[46] V.N. Kuznetsov, N. Serpone, J. Phys. Chem. C 111 (2007) 15277–15288.
[47] J. Zhang, Z. Zhao, X. Wang, T. Yu, J. Guan, Z. Yu, Z. Li, Z. Zou, J. Phys. Chem. C 114 (2010) 18396–18400.